Transient superconductivity in three-dimensional Hubbard systems by combining matrix product states and self-consistent mean-field theory

S. Marten[1], G. Bollmark[2], T. Köhler[2], S.R. Manmana[1], A. Kantian[2,3]

1 Institut für Theoretische Physik, Georg-August-Universität Göttingen, 37077 Göttingen, Germany **2** Department of Physics and Astronomy, Uppsala University, Box 516, S-751 20 Uppsala, Sweden **3** SUPA, Institute of Photonics and Quantum Sciences, Heriot-Watt University, Edinburgh EH14 4AS, United Kingdom

Abstract

We combine matrix-product-state (MPS) and mean-field (MF) methods to model the real-time evolution of a three-dimensional (3D) extended Hubbard system formed from one-dimensional (1D) chains arrayed in parallel with weak coupling in-between them. This approach allows us to treat much larger 3D systems of correlated fermions out-of-equilibrium over a much more extended real-time domain than previous numerical approaches. We deploy this technique to study the evolution of the system as its parameters are tuned from a charge-density wave phase into the superconducting regime, which allows us to investigate the formation of transient non-equilibrium superconductivity. In our ansatz, we use MPS solutions for chains as input for a self-consistent time-dependent MF scheme. In this way, the 3D problem is mapped onto an effective 1D Hamiltonian that allows us to use the MPS efficiently to perform the time evolution, and to measure the BCS order parameter as a function of time. Our results confirm previous findings for purely 1D systems that for such a scenario a transient superconducting state can occur.

Contents

1 Introduction

Superconductivity (SC) has remained a phenomenon of great interest to researchers ever since its discovery in 1911 by H. K. Onnes. Explaining SC in metals at low-temperature equilibrium was already a challenge, taking more than 40 years until the Bardeen-Cooper-Schrieffer (BCS) framework could explain it via a suitable mean-field (MF) theory. In the 1980s, SC at high critical temperatures T_c [1–4] was discovered, which seemed not to be described by BCS theory. In fact, it's theoretical description presents a still-ongoing challenge. It is believed that strongly correlated electron motion is the underlying reason for this type of SC state. Many-body models such as the Hubbard- [5–10] or the t-J-model [4, 10–13] have been investigated to study this question. In more recent developments, experiments claimed to have detected metastable, light-induced SC states after pushing materials out-of-equilibrium in pump-probe setups. Such a transient non-equilibrium SC regime is possibly even detected above the equilibrium critical temperature T_c [14–17]. On the theoretical side, this scenario has been studied in various approaches, e.g., numerically [18–20], but many basic questions about the mechanisms that could lead to dynamically induced superconductivity remain open.

While many experiments rely on the time-dependent optical conductivity as a probe for nonequilibrium SC, Paeckel et al. [19] recently showed that this measure lacks specificity for SC order, at least in the setup studied there. Alternative experimental measures are then proposed, which would be better suited to detecting the onset of the SC state in the dynamically evolving system. The setup studied in that article consists of a quantum quench on a purely one-dimensional (1D) extended Hubbard system using a matrix-product-state (MPS) description.

However, while this MPS approach is unbiased and highly accurate, it is so far largely restricted to 1D systems, especially when treating out-of-equilibrium dynamics. The question is thus if the findings of Paeckel et al. are specific to 1D, with its strong quantum and thermal fluctuations, or whether their results also apply to the realm of higher dimensional systems. This sets an immediate challenge: which theoretical method could address the dynamics of interacting fermions out-of-equilibrium in three-dimensional (3D)?

On their own, even in 1D, MPS methods may require exponentially increasing resources as simulation time grows in order to maintain a set accuracy. This is due to the strong growth in bipartite entanglement in these systems with time: for MPS approaches to be efficient, this entanglement should not be too large. Furthermore, already for equilibrium calculations long-range interactions, which are needed to represent two-dimensional (2D) and 3D systems in 1D, increase the entanglement dramatically. Hence, the time evolution of generic 2D and 3D systems are entirely out of reach for any brute-force MPS-based approach.

For such higher-dimensional systems, real-time non-equilibrium dynamical mean-field theory (DMFT) could be a powerful alternative approach [21, 22]. In these approaches, one or a few lattice sites - the impurity or, respectively, the cluster - are retained explicitly, including all interactions of the original, infinitely-large lattice. In DMFT, the effect of this remainder-lattice on the cluster is mimicked via a free-electron bath that is coupling to it. The parameters of this bath are fixed via self-consistency conditions. Solving these cluster-bath systems within this self-consistency constraint is typically achieved by applying quantum Monte Carlo (QMC) techniques in the real time domain. These techniques suffer from a strong sign-problem, i.e., their numerical error grows exponentially as the cluster-size and the real-time domain, over which the simulation runs, are increased. In practice, a few sites and time scales on the order of the electron tunneling are accessible. Alternatively, MPS solvers can be used within such real-time non-equlibrium DMFT;

however, due to the long-range tunneling in these systems between bath and cluster sites, and the strong growth of entanglement with time, these will also be limited to a few sites and short times.

This leads us to the scope of the present paper: with current methods it seems practically impossible to perform meaningful simulations of dynamically-induced SC in a 3D system. For MPS methods, the growth of entanglement with system size and simulation time is prohibitive, for non-equilibrium real-time DMFT, the large clusters and long times required to resolve the onset of a potentially weak SC order appear out of reach.

However, as we demonstrate in the following, it is possible to make such a specific category of systems amenable to MPS techniques via a static MF ansatz, by exploiting certain gaps in the excitation spectrum of these cases. In this way, it is possible to capture strong correlations by the MPS, and treat the full 3D system more accurately than by applying a pure MF treatment.

Indeed, related approaches have been studied before at equilibrium [23], where at least qualitative behavior was reproduced correctly compared to appropriate QMC simulations [24, 25]. In these approaches, weakly coupled chains or ladders are stacked up into 3D cubic systems, which thus have anisotropic tunneling — much stronger inside the 1D systems than in-between them in the two orthogonal directions. For the case of fermions, the MF approximation can be introduced if each of the constituent 1D systems has a gapped energy sector, such as a spin gap, and thus single-fermion tunneling in-between 1D systems is suppressed in this weak-coupling regime [24]. Just as for the equilibrium case [24], it is this crucial ingredient that allows us to perform real-time evolution for a much higher number of correlated sites than non-equilibrium real-time DMFT, as well as extending the real-time domain enough to perform a meaningful simulation of the dynamically-induced SC in a 3D system. Within this well-behaved domain, we apply our real-time MPS+MF technique to study the time-evolution of the BCS order parameter after fast ramping the system from an insulating starting state into a parameter regime where the system would be SC in equilibrium. As a consequence, we observe the onset of a non-equilibrium SC state.

The paper is structured as follows: In Sec. 2, we recapitulate the MF ansatz for weakly coupled Hubbard chains used in equilibrium, developed originally in [24]. In Sec. 3, we introduce the extension to a self-consistent time-dependent MPS+MF scheme to study the time evolution of a 3D extended Hubbard system, which consists of weakly coupled chains. In Sec. 4, we present our results for the BCS order parameter and a detailed discussion of the convergence behavior of the method when treating 3D arrays formed from chains, each up to $L = 30$ lattice sites long. The time evolution of the SC order parameter shows indeed that in both finite systems as well as the thermodynamic limit a transient SC state can be entered. We further analyze the dependence of our results on the parameters of the simulations. In Sec. 5 we conclude and give an outlook to possible further developments and applications of our method. The appendices discuss further details on the method at equilibrium, as well as further details of the simulations out-of-equilibrium.

2 Mapping of the 3D system onto a 1D self-consistent chain

As we aim to describe a 3D model system with a method that is mainly suitable for 1D, namely MPS, we first need to identify a class of 3D models amenable to mapping onto an effective 1D description. Following the work of Bollmark et al. [24, 25], we focus on 3D systems constructed out of gapped 1D fermions. We arrange these 1D systems, which extend in the $\hat{\mathbf{x}}$-direction, in parallel into a square array in the $\hat{\mathbf{y}} - \hat{\mathbf{z}}$-plane, forming

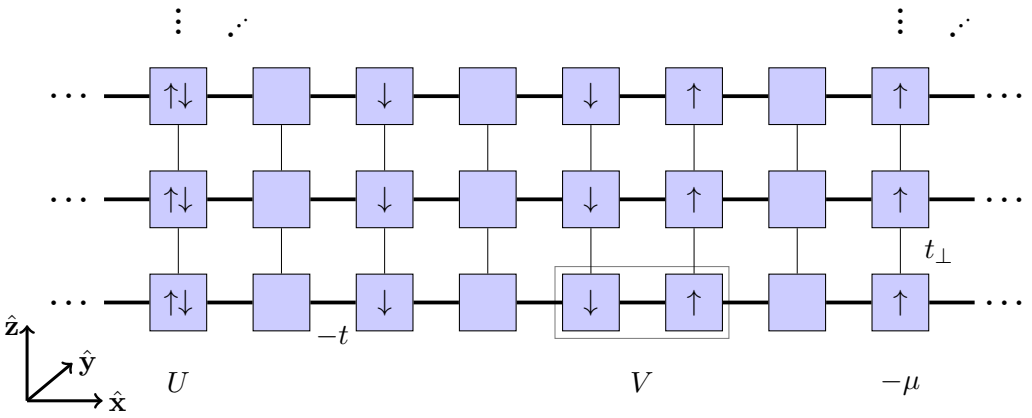

Figure 1: Two-dimensional cross-section of the three dimensional model. For the sake of clarity, the 3D extension of the system out of the plane is not shown here. Each box denotes a lattice site. The sites are coupled to chains in $\hat{\mathbf{x}}$-direction, which is illustrated by the thick lines between the boxes. Furthermore, all chains are weakly coupled by the transverse hopping $t_\perp$. This way, we obtain an extension in $\hat{\mathbf{y}}$ and $\hat{\mathbf{z}}$-direction.

effectively a cubic lattice. We choose fermion tunneling to be anisotropic in this lattice, denoted by $t_\perp$ in the $\hat{\mathbf{y}}$- and $\hat{\mathbf{z}}$-directions. Adapting from Bollmark et al. [24], we choose an extended Hubbard chain as the 1D building block. The Hamiltonian constructed in this manner is illustrated in Fig. 1 and is given by

$$\hat{H} = \hat{H}_0 + t_\perp \hat{H}_\perp \,, \tag{1}$$

with

$$\hat{H}_0 = -t \sum_{n=1}^{L-1} \sum_{\sigma\in\{\uparrow,\downarrow\}} \sum_{\{\mathbf{R}_i\}} \left(\hat{c}^\dagger_{n+1,\mathbf{R}_i,\sigma} \hat{c}_{n,\mathbf{R}_i,\sigma} + \text{h.c.} \right) - \mu \sum_{n=1}^{L} \sum_{\sigma\in\{\uparrow,\downarrow\}} \sum_{\{\mathbf{R}_i\}} \hat{n}_{n,\mathbf{R}_i,\sigma} \tag{2}$$

$$+ U \sum_{n=1}^{L} \sum_{\{\mathbf{R}_i\}} \hat{n}_{n,\mathbf{R}_i,\uparrow} \hat{n}_{n,\mathbf{R}_i,\downarrow} + V \sum_{n=1}^{L-1} \sum_{\sigma,\sigma'\in\{\uparrow,\downarrow\}} \sum_{\{\mathbf{R}_i\}} \hat{n}_{n+1,\mathbf{R}_i,\sigma} \hat{n}_{n,\mathbf{R}_i,\sigma'} \,, \tag{3}$$

and

$$\hat{H}_\perp = -\sum_{n=1}^{L} \sum_{\sigma\in\{\uparrow,\downarrow\}} \sum_{\{\mathbf{R}_i\}} \sum_{\hat{\mathbf{a}}\in\{\hat{\mathbf{y}},\hat{\mathbf{z}}\}} \left(\hat{c}^\dagger_{n,\mathbf{R}_i+\hat{\mathbf{a}},\sigma} \hat{c}_{n,\mathbf{R}_i,\sigma} + \text{h.c.} \right) \,. \tag{4}$$

Here, $\hat{c}^\dagger_{n,\mathbf{R}_i,\sigma}$ and $\hat{c}_{n,\mathbf{R}_i,\sigma}$ denote the fermionic creation and annihilation operators on site n and for spin σ on a chain that is labeled by the index $\mathbf{R}_i$. They obey the anticommutation relations $\{\hat{c}_i, \hat{c}^\dagger_j\} \equiv \hat{c}_i \hat{c}^\dagger_j + \hat{c}^\dagger_j \hat{c}_i = \delta_{ij}$ and $\{\hat{c}_i, \hat{c}_j\} = \{\hat{c}^\dagger_i, \hat{c}^\dagger_j\} = 0$. The indices i and j stand for different combinations of $n, \mathbf{R}_i$, and σ. The operator $\hat{n}_{n,\mathbf{R}_i,\sigma} = \hat{c}^\dagger_{n,\mathbf{R}_i,\sigma} \hat{c}_{n,\mathbf{R}_i,\sigma}$ is the particle number operator for the corresponding site, chain, and spin. We use open boundary conditions and include a term for the chemical potential μ. The latter allows us to control the number of particles in the system.

The only non-1D term is the transverse hopping $\hat{H}_\perp$. We are able to eliminate the beyond-1D nature of this term through a combination of perturbation theory on the transverse hopping and a MF decoupling of adjacent 1D systems. In the following we briefly recap the key steps, a detailed derivation of this approach can be found in the publications of Bollmark et al. [24].

Since we are interested in a model system for SC, we specify $U < 0$ in the chain-Hamiltonian Eq. (3). This negative-U term gives rise to pairing of opposite-spin fermions already in isolated systems at $t_\perp = 0$. This is expressed by the finite spin gap ΔE_s and a finite pairing energy ΔE_p of these isolated chains, defined as follows:

$$\Delta E_s(N) \equiv \mathcal{E}_0(1, N) - \mathcal{E}_0(0, N), \tag{5}$$

$$\Delta E_p(N) \equiv 2\mathcal{E}_0\left(\frac{1}{2}, N+1\right) - \mathcal{E}_0(0, N) - \mathcal{E}_0(0, N+2)\ . \tag{6}$$

Here, $\mathcal{E}_0(S_z, N)$ denotes the ground-state energy of Hamiltonian $\hat{H}_0$ for a single chain-index at total spin S_z and total number of fermions N. Thus, ΔE_s and ΔE_p represent the minimal energy required for flipping a spin inside a chain and for breaking up a pair on a chain by moving one constituent to another chain in the full 3D system, respectively. From the definitions, it is easy to see that $\Delta E_s \leq \Delta E_p$, and for our specific choice of 1D systems $\Delta E_s = \Delta E_p$. As outlined in the following, ΔE_p becomes important in the actual numerical routine, directly entering the effective Hamiltonian Eq. (13). In practice, we can determine ΔE_p from a single chain via an extrapolation in the system size $L \to \infty$.

To carry out the second-order perturbation theory in $\hat{H}_\perp$ – specifically in $t_\perp/\Delta E_p$ – we follow [26]. We sort the eigenenergies $E_{i,\alpha}$ of $\hat{H}_0$, i.e., $\hat{H}_0 \left|i, \alpha\right\rangle = E_{i,\alpha} \left|i, \alpha\right\rangle$, into a lowest-energy manifold $E_{i,\alpha=0}$, where i indexes the states within this manifold. In this manifold, there are no broken pairs. The high-energy manifold $E_{i,\alpha=1}$ is at least ΔE_p above the low-energy manifold, corresponding to excited states with at least one broken pair, i.e., where the pair-constituents have moved onto separate chains. In the perturbative regime, we thus assume

$$|E_{i,\alpha} - E_{j,\alpha}| \ll |E_{i,\alpha} - E_{j,\beta}|; \quad \alpha \neq \beta \tag{7}$$

to hold.

We therefore target a small transverse hopping strength $t_\perp$ with respect to ΔE_s and ΔE_p. Introducing the projector onto the lowest-energy manifold $\hat{P}_0 = \sum_i \left|E_{i,0}\right\rangle\left\langle E_{i,0}\right|$, the second-order perturbation theory for Hamiltonian Eq. (1) yields:

$$\hat{H}^0_{\text{eff}} = \hat{P}_0 \hat{H}_0 \hat{P}_0 - \frac{t_\perp^2}{\Delta E_p} \hat{P}_0 \hat{H}_\perp^2 \hat{P}_0\ . \tag{8}$$

Written explicitly, $\hat{H}_\perp^2$ is

$$\begin{aligned}\hat{H}_\perp^2 = &\sum_{n,m=1}^{L} \sum_{\sigma\in\{\uparrow,\downarrow\}} \sum_{\{\mathbf{R}_i\}} \sum_{\hat{\mathbf{a}}\in\{\hat{\mathbf{y}},\hat{\mathbf{z}}\}} \left(\hat{c}^\dagger_{n,\mathbf{R}_i+\hat{\mathbf{a}},\sigma} \hat{c}_{n,\mathbf{R}_i,\sigma} \hat{c}^\dagger_{m,\mathbf{R}_i+\hat{\mathbf{a}},-\sigma} \hat{c}_{m,\mathbf{R}_i,-\sigma} + \text{h.c.}\right) \\ &+ \sum_{n,m=1}^{L} \sum_{\sigma\in\{\uparrow,\downarrow\}} \sum_{\{\mathbf{R}_i\}} \sum_{\hat{\mathbf{a}}\in\{\hat{\mathbf{y}},\hat{\mathbf{z}}\}} \left(\hat{c}^\dagger_{n,\mathbf{R}_i+\hat{\mathbf{a}},\sigma} \hat{c}_{n,\mathbf{R}_i,\sigma} \hat{c}^\dagger_{m,\mathbf{R}_i,\sigma} \hat{c}_{m,\mathbf{R}_i+\hat{\mathbf{a}},\sigma} + \text{h.c.}\right) \qquad (9) \\ =&\hat{H}_{\text{pair}} + \hat{H}_{\text{exc}}\ . \qquad (10)\end{aligned}$$

Within Eq. (10), we identify two contributions, namely a pairing term $\hat{H}_{\text{pair}}$, which denotes the hopping of electron-electron pairs of opposite spin between neighboring chains and an exchange term $\hat{H}_{\text{exc}}$, denoting the exchange of particles of the same spin between neighboring chains.

In the following we use MF theory to eliminate the non-1D nature of $\hat{H}_\perp^2$. Here, we make use of the relation

$$c_i^{(\dagger)} c_j^{(\dagger)} = \left(c_i^{(\dagger)} c_j^{(\dagger)} - \langle c_i^{(\dagger)} c_j^{(\dagger)} \rangle\right) + \langle c_i^{(\dagger)} c_j^{(\dagger)} \rangle\ , \tag{11}$$

and assume $\left(c_i^{(\dagger)}c_j^{(\dagger)} - \langle c_i^{(\dagger)}c_j^{(\dagger)}\rangle\right)$ to be small. We, moreover, assume

$$\langle \hat{c}_{n,\uparrow}\hat{c}_{m,\downarrow}\rangle = \langle \hat{c}_{n,\mathbf{R}_i,\uparrow}\hat{c}_{m,\mathbf{R}_i,\downarrow}\rangle = \langle \hat{c}_{n,\mathbf{R}_i+\hat{\mathbf{a}},\uparrow}\hat{c}_{m,\mathbf{R}_i+\hat{\mathbf{a}},\downarrow}\rangle \ , \tag{12}$$

which means that all the chains are exact copies of each other. We end up with an effectively 1D expression for a Hamiltonian describing a higher-dimensional model, namely

$$\begin{aligned}\hat{H}_{\text{eff}}^{\text{MF}} =& \hat{H}_0 - \sum_{n,m=1}^{L}\left(\alpha_{n,m}^{*}\hat{c}_{n,\uparrow}\hat{c}_{m,\downarrow} + \alpha_{n,m}\hat{c}_{m,\downarrow}^{\dagger}\hat{c}_{n,\uparrow}^{\dagger}\right) \\ &+ \sum_{n=1}^{L}\sum_{\sigma\in\{\uparrow,\downarrow\}}\sum_{r=1}^{L-n}\left(\beta_{n,r,\sigma}^{*}\hat{c}_{n+r,\sigma}^{\dagger}\hat{c}_{n,\sigma} + \beta_{n,r,\sigma}\hat{c}_{n,\sigma}^{\dagger}\hat{c}_{n+r,\sigma}\right)\end{aligned} \tag{13}$$

with

$$\alpha_{n,m} = \frac{2z_c t_\perp^2}{\Delta E_p}\langle \hat{c}_{n,\uparrow}\hat{c}_{m,\downarrow}\rangle \quad \text{and} \tag{14}$$

$$\beta_{n,r,\sigma} = \frac{2z_c t_\perp^2}{\Delta E_p} v\,\langle \hat{c}_{n+r,\sigma}^{\dagger}\hat{c}_{n,\sigma}\rangle \ , \tag{15}$$

and thus identify $\alpha_{n,m}$ with the MF-approximated pairing part of Eq. (10) and $\beta_{n,r,\sigma}$ with its exchange part. Here, we introduced the coordination number z_c, which denotes the number of neighboring chains. In our case $z_c = 4$, as the chains are assembled into a 2D square grid in the $\hat{\mathbf{y}} - \hat{\mathbf{z}}$-plane. The parameters $\alpha_{n,m}$ and $\beta_{n,r,\sigma}$ are the so-called MF parameters, meaning they need to be calculated self-consistently for all times. The work in [24] explains this for the ground state and for the finite-temperature equilibrium of the 3D system. There, the authors demonstrate that the MPS+MF approach for equilibrium systems produces the correct physics compared against QMC, in regimes in which the latter approach is quasi-exact, in a negative-U Hubbard model on a 2D square lattice with anisotropic tunneling. That work also shows that the error in T_c for the SC state due to the MF approximation within the MPS+MF framework is a quasi-constant one in $t_\perp$ over a significant range. Moreover, at zero temperature, the overestimation of the SC order parameter becomes systematically better as $t_\perp$ decreases.

Based on the good performance of the MPS+MF scheme in equilibrium, the present work is concerned with the performance of the self-consistent evaluation of the MF parameters Eq. (14) and Eq. (15) for a time-evolving system.

Since the present work aims to test and benchmark the method itself, in the following we are working with the simplest possible version of the Hamiltonian Eq. (13). We neglect the exchange term $\beta_{n,r,\sigma}$ and allow only for site-independent onsite pairing, meaning $\alpha_{n,m} \equiv \alpha_{n,n} \equiv \alpha$. This leads to

$$\hat{H}_{\text{eff}}^{\text{MF}} = \hat{H}_0 - \sum_{n}\left(\alpha^{*}\hat{c}_{n,\uparrow}\hat{c}_{n,\downarrow} + \alpha\hat{c}_{n,\downarrow}^{\dagger}\hat{c}_{n,\uparrow}^{\dagger}\right) \tag{16}$$

with

$$\alpha = \frac{1}{L}\frac{2z_c t_\perp^2}{\Delta E_p}\sum_{n=1}^{L}\langle \hat{c}_{n,\uparrow}\hat{c}_{n,\downarrow}\rangle \ . \tag{17}$$

In this last expression we are adapting the evaluation of the order parameter α to the open boundary conditions. Obtaining α from an average across the entire system removes the spatial variation that is solely due to these open boundaries.

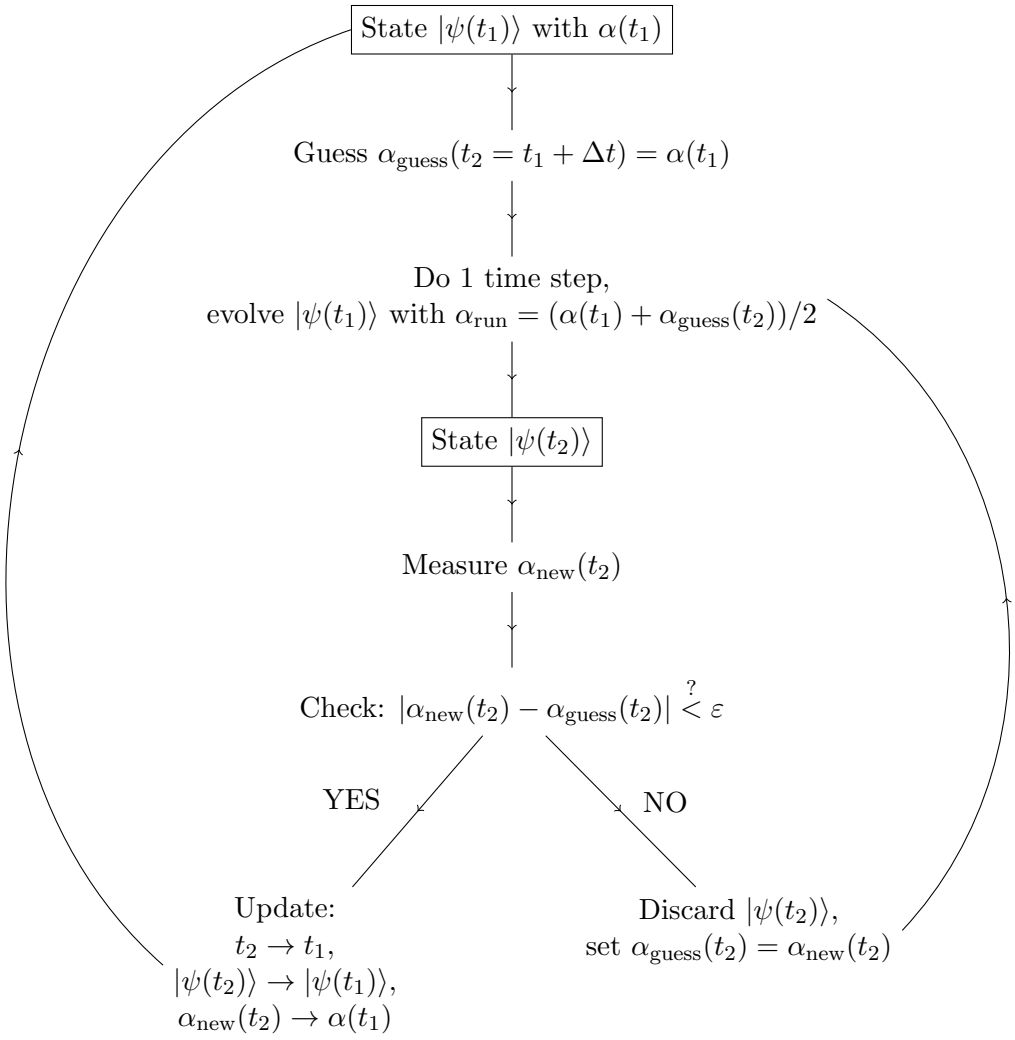

Figure 2: Self consistency loop for one time step. As the MF-parameter α depends on the state itself, a continuous adjustment of it is required.

3 MPS+MF-Algorithm for self-consistent time-evolution

The expectation values needed to compute the MF parameter α in Eq. (17) are computed using a self-consistent scheme for both the time-evolution and for the ground-state search of our model system. In this section a schematic description of the time-evolution routine is presented, which is one of our main results. The algorithm is based on the work of H. Strand et al. published in [27], where a non-equilibrium version of real-time DMFT for bosons is introduced. Our work incorporates this real-time scheme into a MPS framework and adapts it to 3D lattices of correlated fermions built from weakly coupled 1D systems. All results obtained in the following were generated with Ian McCulloch's matrix product toolkit [28]. The initial ground states from which the time evolution proceeds were generated from a self-consistent scheme introduced by Bollmark et al. in [25], which is also briefly described in App. A.

At the beginning of each time step, we start with a state $|\psi(t_1)\rangle$ at time t_1, which we already have obtained before (either as a previous step or as initial state). From this state, we measure the value of the MF parameter $\alpha(t_1)$. Now, we guess which value α might take after one discrete time step dt. In this work, at the start of the self-consistency iterations

for each time step, we just assume that the α value does not change at all. In any case, the guess for α at $t_2 = t_1 + \mathrm{d}t$, is labeled $\alpha_{\mathrm{guess}}(t_2)$. Then, we evolve the system from t_1 to t_2 using the mean of $\alpha(t_1)$ and α_{guess}. From the resulting tentative $|\psi(t_2)\rangle$ we can once again measure the MF parameter $\alpha_{\mathrm{new}}(t_2)$. Next we calculate the distance between the measured and the guessed value and compare it to a chosen precision ε,

$$|\alpha_{\mathrm{new}}(t_2) - \alpha_{\mathrm{guess}}(t_2)| < \varepsilon \quad \text{with} \quad \varepsilon \ll 1 \,. \tag{18}$$

If Eq. (18) is fulfilled, we keep the state $|\psi(t_2)\rangle$ and proceed with the next time step. Otherwise, we discard $|\psi(t_2)\rangle$ and repeat the time step using the mean of $\alpha(t_1)$ and $\alpha_{\mathrm{new}}(t_2)$. The loop is repeated until Eq. (18) is fulfilled. A schematic of the algorithm is depicted in Fig. 2.

4 Transient SC after a fast ramp of the nearest-neighbor interaction

In this section, we present our results using the self-consistent MPS+MF scheme and find that in the extended Hubbard model Eq. (1) the BCS order parameter for SC grows in time and begins to oscillate around a finite value on the treated time scales. This indicates the formation of transient SC, which is the second main result of this paper. In the following, all parameters are measured in units of the hopping parameter $t \equiv 1$.

More specifically, we follow Paeckel et al. [19] and tune the system's parameters from a charge-density wave (CDW) phase into a SC phase. However, we find that the sudden quench performed in [19] is numerically less stable within the self-consistent scheme (see App. B), so we instead perform a fast ramp.

In order to check the equilibrium phases of the 3D model we use the self-consistent MPS+MF approach to compute the ground states using the routine introduced by Bollmark et al. [25] for different parameters and measure the expectation value of the MF parameter α. We find that for $t_\perp = 0.2$, $U = -4$ and $V = 0.25$ the system possesses the main properties of a CDW phase relevant for us, i.e., we find alternating occupation of the lattice sites by the electrons and a vanishing value of α. For $U = -4$ and $V = -0.25$ instead, the system is SC, as here $\alpha \sim 10^{-1}$ becomes finite and density oscillations less pronounced. These are the same parameters treated by Paeckel et al. in [19] for the purely 1D system. Hence, we perform a fast ramp by tuning the values of the nearest-neighbor interaction from $V = 0.25$ to $V = -0.25$ as further detailed below.

Since the effective Hamiltonian Eq. (16) depends on the MF parameter $\alpha(t)$ the question of how to choose $\alpha_{\mathrm{ini}} := \alpha(t = 0)$ arises. For the CDW system $\alpha = 0$ and it is hence difficult for it to grow with the method outlined in Fig. 2. Because of this, unless otherwise noted, our default value for this work is $\alpha_{\mathrm{ini}} = 10^{-4}/\mathrm{d}t$, where $\mathrm{d}t$ is the size of the discretized time step of the simulation. Such a small yet finite value is justified by the fact that any system will either have a microscopic fraction of pairs in the center-of-mass zero-momentum state to begin with, or such a fraction is generated during the ramp or quench. Scaling α_{ini} inversely in $\mathrm{d}t$ ensures that simulations with different $\mathrm{d}t$ agree over long times, see Fig. 3.

The MF term of the Hamiltonian causes the effective model to be no longer particle-number conserving, hence, we need to adjust the value of the chemical potential μ corresponding to the system size and to the onsite repulsion U in order to fix the average density of the total system. From the ground-state calculations we find the values of μ that are listed in table 1. We keep the values of μ, determined in this manner, fixed throughout the whole time evolution in order to keep our algorithm simple and stable. However, we

Table 1: List of values for the chemical potential μ to obtain half filling for $U = -4.0$ and $V = \pm 0.25$ for various system sizes L.

L	12	20	30
$\mu(V = -0.25)$	-2.44	-2.47	-2.48
$\mu(V = 0.25)$	-1.66	-1.63	-1.62

still need to keep track of the overall density of our system during the time evolution to check if this assumption of a time-independent chemical potential is justified. Indeed, for our simulations, the value of the density is preserved to a good accuracy over the time scales treated by us (see Figs. 3 and 4). In general, however, it might be necessary to also include a variation of μ into the self-consistency scheme.

4.1 Time evolution of the BCS order parameter and of the total energy

In the following, we investigate the time evolution of the BCS order parameter $\alpha(t)$ (see Eq. (17)) and of the total energy $E(t)$ of the system. The latter cannot be expected to remain constant as the MF term changes the Hamiltonian Eq. (16) during evolution. In addition, we monitor the total density of the system, which should stay at a value of $\rho = 1$ (half filling) during the whole time evolution.

Since we find fast ramps to have lower errors over the simulated time windows than instantaneous quenches, we linearly decrease the value of the nearest-neighbor interaction V from $V = 0.25$ to $V = -0.25$ within a time window of $\Delta t_{\text{ramp}} = 3.0$. A more detailed discussion of the effect of the size of the time window Δt_{ramp} can be found in App. B. In Fig. 3 we see the results for a 30-site system for an evolution up to time $t_{\text{end}} = 50$. Since $\alpha(t)$ is complex-valued we show the evolution of the magnitude $|\alpha(t)|$ and of the phase $\varphi(t)$ of the order parameter in Figs. 3 to 5. We find that $|\alpha(t)|$ grows up to time $t \sim 45$ to a value of approximately $|\alpha| \approx 0.06$, which is clearly non vanishing and hence indicates the formation of a non-equilibrium SC state. In contrast, if we consider a time evolution without a quench or ramp, i.e., $V = 0.25$ during the whole evolution, the value of α stays unchanged at an order of magnitude of 10^{-5} throughout the whole time evolution as can be seen by the dotted blue lines in Fig. 3. The phase $\varphi(t)$ decreases as long as V is decreasing, then oscillates around a value of approximately $\varphi(\alpha)/\pi \approx -0.8$ and seems to increase again slightly when $|\alpha|$ has reached its maximum. We interpret this behavior as an expression of a Josephson effect in-between 1D chains to the extent it can be captured by a single 1D system with time-evolving MF amplitudes. As a kernel of SC order manifests itself in the different chains of the 2D array the macroscopic phases of SC states, within each chain, will be initially uncorrelated, then start aligning via the Josephson effect. With density fluctuating within each individual chain the Josephson effect will keep the phase fluctuating while the system finds a new equilibrium after the rapid ramp, as Fig. 3b shows.

In Fig. 3d we show the evolution of the total energy per site $E(t)/L$ and in Fig. 3e the deviation of the total density $\rho(t)$ from the desired value $\rho_{\text{target}} = 1$. We find that this deviation is of the order of $3 \cdot 10^{-5}$ or smaller for all the times treated, indicating that keeping the chemical potential μ fixed leads only to small errors. The total energy per site E/L behaves as expected during the ramp and decreases almost linearly for the duration of the ramp. Afterwards, we first observe a nearly constant behavior, then a strong decrease until a minimum at time $t \approx 45$, shown in the inset of Fig. 3a. We read the behavior of $E(t)/L$, especially at long times, as the system starting to further lower its energy through condensing Cooper pairs, as the drop in $E(t)/L$ coincides markedly with

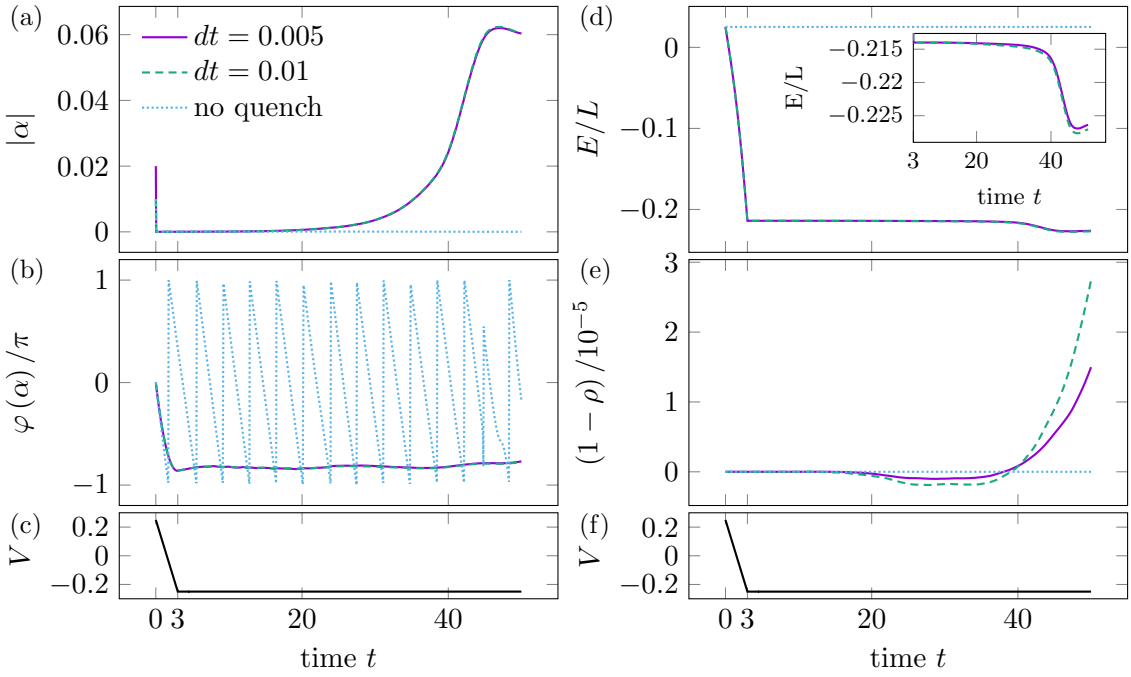

Figure 3: Evolution of the considered parameters in time during and after a ramp on a 30-site system. The plots at the bottom ((c) and (f)) show the nearest-neighbor interaction, which decreases from $V = 0.25$ to $V = -0.25$ during a time window of $\Delta t_{\text{ramp}} = 3.0$. Evolution of the MF parameter α split up into magnitude (a) and phase (b). Evolution of the total energy per site of the system (d) and the total density (e). The inset in (d) shows the evolution of the energy per site after V was decreased. The legend is valid for all plots. All the data shown here were obtained with a bond dimension of $\chi = 250$, an initial guess of the MF parameter of $\alpha_{\text{ini}} = 10^{-4}/\mathrm{d}t$, and the chemical potential was taken from table 1. We compare the ramp scenario (solid violet and dashed green) with an evolution during which we keep the nearest neighbor interaction at $V = 0.25$ constant (dotted blue). For the latter calculation we chose a time step of $\mathrm{d}t = 0.01$.

the onset of a finite value of $\alpha(t)$. We also study the effect of system size, to make certain the dynamical onset of superconductivity would survive in the thermodynamic limit. In Fig. 4 we compare the results for different chain lengths L. From these, we extract the instant t_{SC}, at which $|\alpha(t)|$ reaches its first maximum. The data of the 12-site system shows the onset of oscillation for $|\alpha(t)|$ around a finite value, indicating a dynamically induced SC phase (longer-time simulations for $L = 12$ further confirm this, as shown in Figs. 5 to 7 for times up to $t_{\text{max}} = 100$). The inset of Fig. 5a displays an extrapolation in inverse chain length $1/L$ of t_{SC}. In order to see whether t_{SC} diverges we performed a quadratic and a linear fit, both indicating a finite value in the limit $L \to \infty$. Since for the larger system sizes $|\alpha(t)|$ starts to oscillate at around the maximal time reached by us, it is difficult to obtain a finite-size extrapolation of the value of the SC order parameter. In order to do so, one needs to extend the simulations for the larger systems to substantially longer times, which is beyond the scope of this paper.

4.2 Accuracy of results and sensitivity to simulation parameters

The results so far were all obtained using the same parameters for the self-consistency cycle. In the following we study how sensitive the results are on parameters like the initial guess of the MF parameter α_{ini} (see Sec. 3), the bond dimension of the MPS calculations,

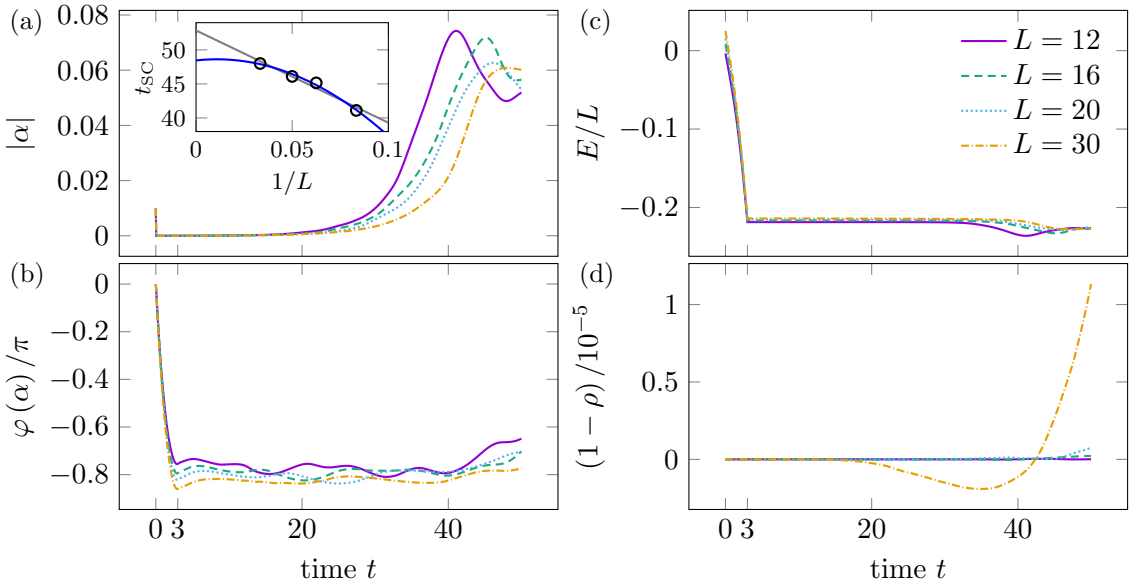

Figure 4: Evolution of SC order-parameter α, energy per site E/L, and density ρ in time during and after a ramp for sizes $L = 12, 16, 20, 30$. Magnitude and phase of α are shown in (a) and (b), respectively. The inset in (a) shows the time at which the first local maximum in $|\alpha|$ occurs plotted against the inverse of the system size $1/L$. Both, the linear and the quadratic fit suggest a finite and comparable value of t_{SC} in the limit $L \to \infty$. Evolution of the total energy of the system and the total density are shown in (c) and (d). All data were obtained with a bond dimension of $\chi = 500$, an initial guess of the MF parameter of $\alpha_{\mathrm{ini}} = 10^{-4}/\mathrm{d}t$, a ramp time window $\Delta t_{\mathrm{ramp}} = 3$, and the chemical potential was taken from table 1.

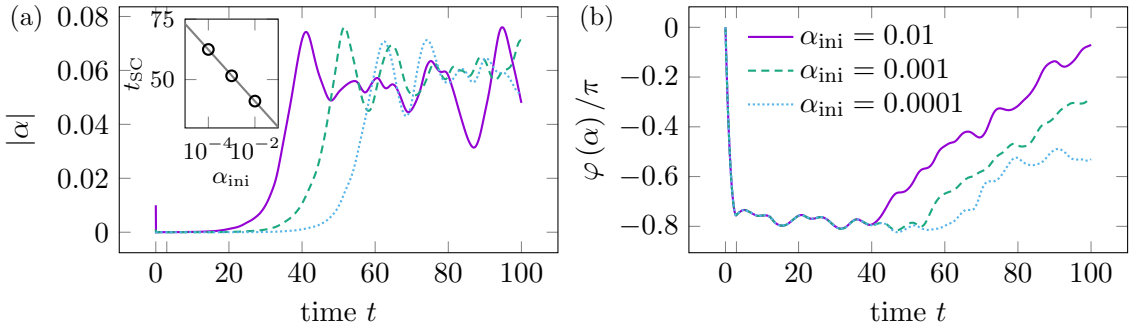

Figure 5: Evolution of the MF parameter α split up into its magnitude (a) and its phase (b) for different initial guesses α_{ini} in a 12-site system. We see that the reduction of α_{ini} induces merely a shift in the data, at least up to time t_{SC} at which the first maximum of $|\alpha|$ occurs. The inset in (a) shows t_{SC} vs. α_{ini} and a linear fit on a semilogarithmic scale. This shows that t_{SC} grows merely logarithmically with α_{ini}. The data shown was obtained with $\chi = 500$ and $\mathrm{d}t = 0.01$, a ramp time window $\Delta t_{\mathrm{ramp}} = 3$, and μ was taken from table 1.

or the discrete time step $\mathrm{d}t$. To study these effects, we focus on the 12-site system in order to reach the longest time scales.

Figure 5 shows the evolution of the magnitude and phase of $\alpha(t)$ for different initial values α_{ini}. Decreasing the value of α_{ini} induces a shift of t_{SC} to later times. In order to further analyze this, we plot the value of t_{SC} against the value of α_{ini} in the inset of

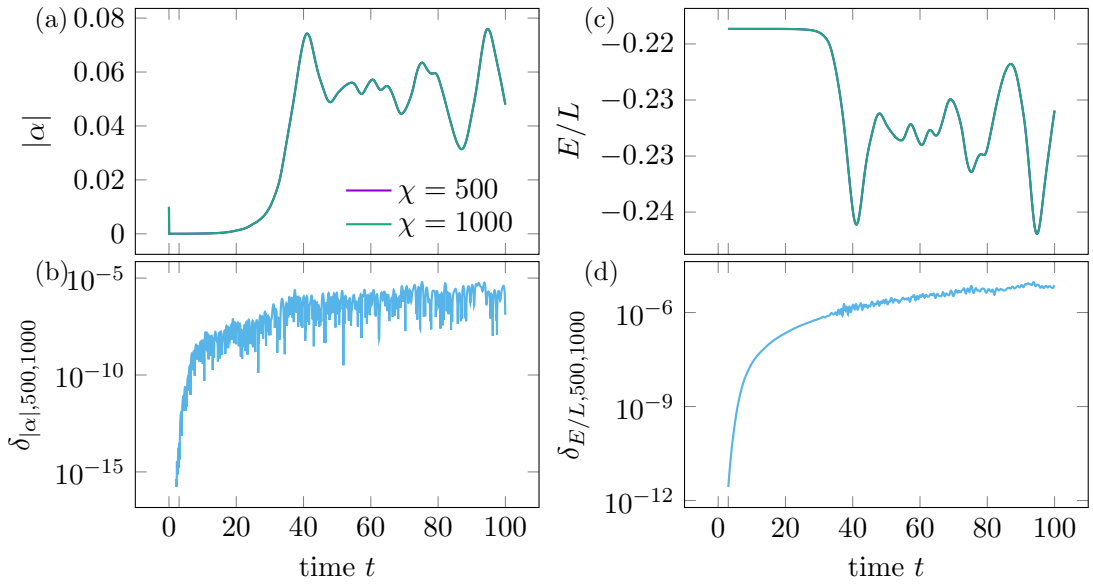

Figure 6: Evolution of (a) the magnitude of the MF parameter $|\alpha|$ and (c) the total energy E for two different bond dimensions $\chi_1 = 500$ and $\chi_2 = 1000$ in a 12-site system. (b) and (d) show the difference $\delta_{\mathcal{O},\chi_1,\chi_2}$ between the observables we measure for these two different bond dimensions. All calculations were done with $\alpha_{\text{ini}} = 10^{-4}/\mathrm{d}t$, a ramp time window $\Delta t_{\text{ramp}} = 3$, and $\mathrm{d}t = 0.01$.

Fig. 5a. Speaking to the soundness of our MF approximation, we find that t_{SC} increases only very weakly with α_{ini}, i.e., logarithmically. While this indicates a diverging time for the onset of SC order in the limit $\alpha_{\text{ini}} \to 0$, this is merely consistent with $\alpha_{\text{ini}} = 0$ being an unstable fix point of the dynamic MF algorithm in the regime we ramp into. But any finite value, even a microscopic one, will yield dynamically induced SC order in finite time when ramping into the SC parameter regime. As argued at the outset of Sec. 4: on general physical grounds there will always be some electron pairs whose center-of-mass momentum is zero.

In Fig. 3 we compare two different discretized time steps, $\mathrm{d}t = 0.005$ and $\mathrm{d}t = 0.01$, respectively. The results are nearly identical, only a small deviation of the total density, which agrees up to $\sim 10^{-5}$, can be seen in Fig. 3e.

Regarding the discarded weight of our simulations, we find that even for the smallest bond dimension these values stay below 10^{-6} within the time domains we consider. Nevertheless, we examine the dependence of our results on the MPS bond dimension χ. For this purpose we compute the deviation of the value of an observable $\mathcal{O}$ for two different values of χ,

$$\delta_{\mathcal{O},\chi_1,\chi_2} = |\mathcal{O}(\chi_1) - \mathcal{O}(\chi_2)| \ . \tag{19}$$

At any fixed value of α_{ini} and $\mathrm{d}t$ we find this to be the most reliable estimator for the accuracy of our combined MPS+MF approach (assuming the latter parameter is chosen to be sufficiently small) and focus in the following on this quantity.

In Figs. 6 and 7 we present results for the observables $|\alpha(t)|$ and $E(t)$ obtained with two different bond dimensions $\chi_1 = 500$ and $\chi_2 = 1000$ for the 12-site system, and for $\chi = 250$ and $\chi = 500$ for the 30-site system, respectively, and also the difference of the respective results. For the larger system it was necessary to substantially reduce the values of χ, since otherwise the numerical expenses would exceed the available resources. We find that the deviation of the results is $\sim 10^{-6}$ for the values of $|\alpha(t)|$ and $\sim 10^{-4}$ for the total energy

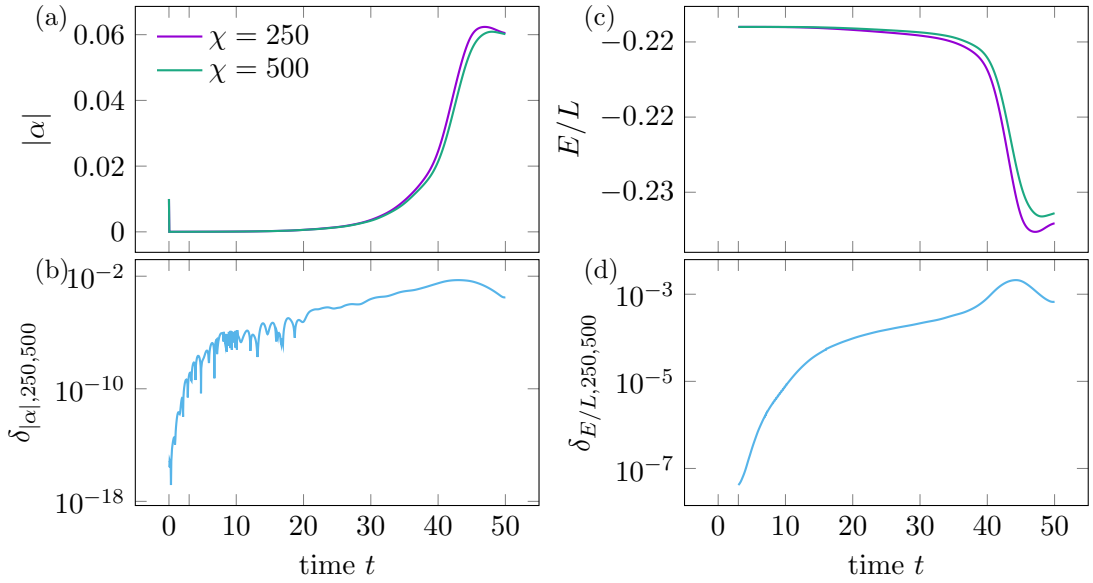

Figure 7: Analog to Fig. 6 but for a 30-site system and for bond dimensions $\chi_1 = 250$ and $\chi_2 = 500$.

$E(t)$, in the case of the 12-site system. For both observables, this is small compared to the order of magnitude of the observables themselves, so that we conclude these values of χ suffice to provide quantitatively accurately results, within the dynamical MPS+MF framework.

For the 30-site system, however, the deviation is $\sim 10^{-3}$ for $|\alpha(t)|$ and $\sim 10^{-2}$ for $E(t)$. This is rather large in comparison to the order of magnitude of the observables themselves. The data obtained from these calculations is hence only trustworthy in regards to the qualitative physics, but for the larger chain lengths one needs a larger bond dimension to obtain a better quantitative convergence of the results.

5 Conclusion

This work presents a self-consistent real-time MPS+MF approach for investigating the time evolution of a 3D extended Hubbard model after a fast ramp. By combining perturbation theory with a MF ansatz, we construct an effective 1D Hamiltonian Eq. (13) capable of capturing the dynamical build-up of SC correlations for this 3D model system, when quenching or rapidly ramping into a Hamiltonian parameter regime corresponding to SC order in equilibrium. This approach is generic to any 3D system composed out of gapped 1D systems of fermions, as long as coupling between 1D systems is sufficiently weak for single-fermion tunneling in-between 1D systems to be suppressed. For concrete demonstration of the performance of this approach, we chose systems of 1D extended Hubbard chains, arranged in parallel in a 2D square array, forming a 3D system with weak interchain tunneling $t_\perp$, negative onsite repulsion U, and nearest-neighbor interaction V along each chain.

We benchmark the self-consistent algorithm introduced on the simplest possible version Eq. (16) of the resulting effective MF Hamiltonian, only taking onsite pairing into account and neglecting the particle-hole terms Eq. (15). We test our approach on systems where each chain is up to $L = 30$ sites long. Using this algorithm we compute the time evolution of the BCS order parameter for SC order $\alpha(t)$, as a direct indicator of dynamically induced

superconductivity. The results show that SC order sets in after a fast ramp from $V = 0.25$ to $V = -0.25$, where the initial V-value realizes an insulating CDW state, and the final value would correspond to SC order at equilibrium. These results are broadly comparable to previous 1D results [19] and represent a best-case scenario, in which double occupancies already present in the CDW help to form the non-equilibrium SC state after the ramp.

Performing infinite-size extrapolations and studying the effect of the microscopic initial kernel of SC order α_{ini} shows that dynamically induced superconductivity is not merely a trivial size effect, but actually present in the thermodynamic limit, and even the smallest yet finite magnitude for α_{ini} will result in establishing order within a finite window of time. At the same time, we find that resource requirements increase substantially with chain length L, but several tens of sites and time frames between one and two orders of magnitude in units of inverse fermion tunneling t^{-1} are accessible already with the modest resources employed for the present proof-of-principle work.

The present work presents multiple avenues for interesting and potentially valuable follow-up work. One of these would be to move towards a regime that is physically more realistic as far as solid state systems are concerned, in which the pair-binding energies ΔE_p would be significantly smaller than in the present work. This would entail either lowering U, or working directly with a 1D model offering repulsively mediated pairing, such as a doped two-leg Hubbard ladder [29, 30]. This would require retaining more particle-particle terms Eq. (14) than we have done for the present proof-of-principle, as well as incorporating the particle-hole terms Eq. (15) into the self-consistent time-evolution step, see Fig. 2. This would be straightforward, as a generic ansatz for the first iteration of these terms is practically imposed by the physics of these 1D systems. As detailed in, e.g., [31], both classes of terms decay with an exponential envelope function characterized by the spin-correlation length, which in turn is easy to obtain from static correlators via density-matrix renormalization group (DMRG) [32, 33] calculations for the isolated systems.

With this extension, the present work could stimulate a more direct and fruitful collaboration between theory and experiment on dynamically induced SC order in solid state systems. Such work would start from either identifying existing materials comprised of many 1D systems of paired electrons in parallel, with coupling weaker than that pairing, or synthesizing such materials. The theory presented in the present work would then allow to closely model any experiments on driving dynamically induced superconductivity in these systems, and thus be much better positioned to ascertain whether some experimental measurement truly is a hallmark of a transient superconducting state, and in turn to propose measurements that would prove the existence of such a state. Regarding such a modeling of realistic solid state systems, we point out that MPS-based techniques are capable of modeling the equilibrium and dynamical out-of-equilibrium evolution of much more complex 1D systems than the one studied in the present work. This includes coupling to phonon baths [34–36] and multi-orbital systems [37], and for spin systems MPS+MF techniques have already been used to model experiments of 3D systems comprised of weakly coupled spin ladders [38, 39].

At the same time, we point out that existing experiments on ultracold atomic gases confined in optical lattices offer an invaluable platform to validate the MPS+MF theory for dynamically induced SC states, in both the high-U and the low-U regime. Systems with all the essential elements of the set-up of this work — anisotropic 3D cubic lattices with $t_\perp/t \ll 1$, $U < 0$ — can readily be realized in the laboratory. These set-ups would thus allow for a direct one-to-one comparison of theory and experiment. Such work would advance the field of out-of-equilibrium many-body dynamics simultaneously on both fronts, as well as establish ultracold atoms as clean, highly controlled model systems of

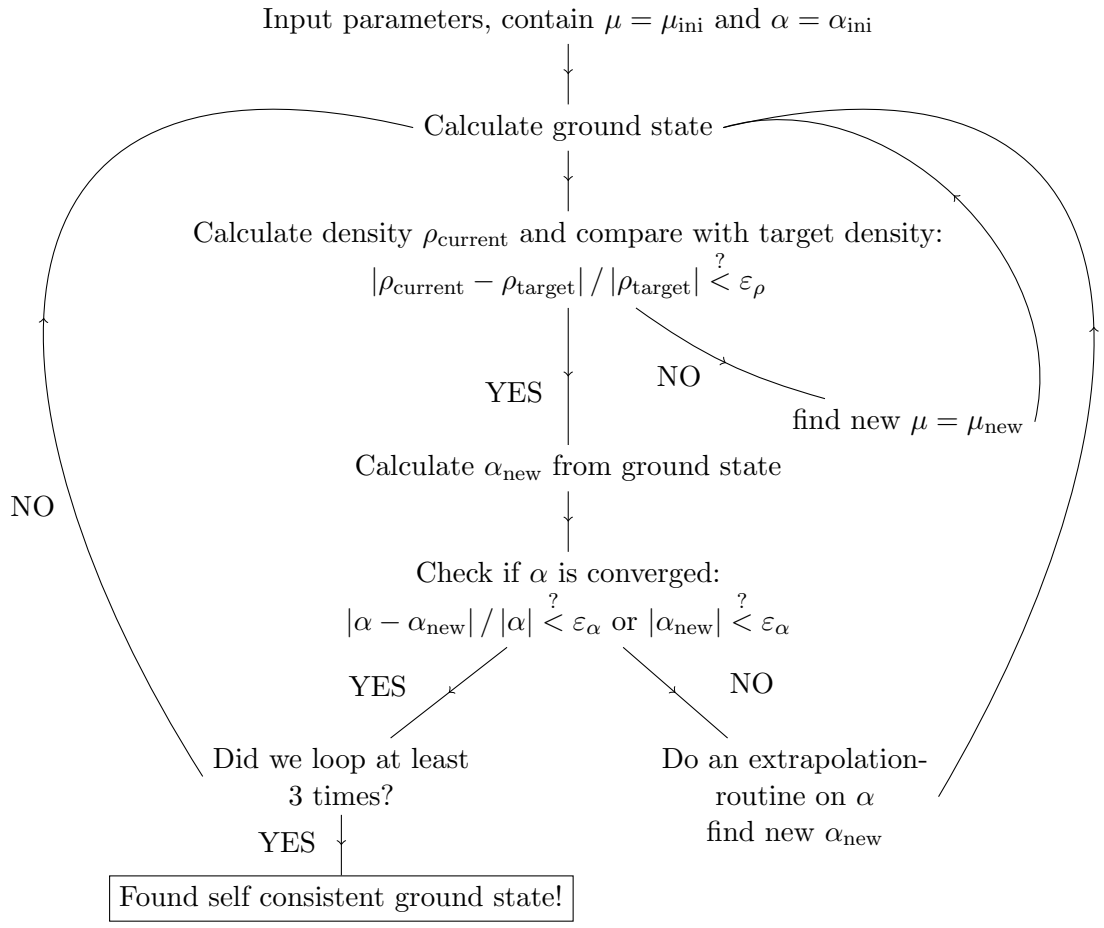

Figure 8: Self consistency loop for the ground-state search. As the MF-parameter α depends on the ground state itself, it has to be adjusted after each DMRG step. As the effective Hamiltonian, furthermore, is no longer particle number conserving we also need to update the chemical potential μ continuously.

dynamically induced SC order.

Acknowledgements We acknowledge helpful discussions with Hugo Strand, Sebastian Paeckel, and Oscar Grånäs. We acknowledges financial support by the ERC Starting Grant from the European Union's Horizon 2020 research and innovation program under grant agreement No. 758935. SRM and SM acknowledge funding by the Deutsche Forschungsgemeinschaft (DFG, German Research Foundation) - 217133147/SFB 1073, project B03 and TU Clausthal. We also acknowledge access to computational resources provided by the GWDG. This work also used the Cirrus UK National Tier-2 HPC Service at EPCC (http://www.cirrus.ac.uk) funded by the University of Edinburgh and EPSRC (EP/P020267/1).

A Self Consistent Ground State Search

As mentioned in Sec. 4 of this paper, we are making use of the self-consistent ground-state search developed by Bollmark et al. [24, 25]. Here a brief description of this algorithm shall be given.

Basically, a ground-state search in MPS language is an optimization problem solved via DMRG. However, in our case we are dealing with the special case that not only the state $|\psi\rangle$ has to be optimized but that we also do not know all parameters of the Hamiltonian as one of the parameters, namely α, depends on the ground state itself. This is why we need to adjust this parameter iteratively during the ground-state search until self consistency is reached, as in any other MF-based approach. By introduction of the α-term in our MF-Hamiltonian, the model loses the particle-number conservation of the original 3D Hamiltonian. Thus, not only α but also the chemical potential μ has to be adjusted during the ground-state search.

At the inception of the iterative procedure α and μ must be guessed, however crudely. Then, we perform a DMRG-based ground-state search for this set of parameters, yielding a candidate for a ground state. Now, we need to check if the density is at the desired value and if α is consistent. First, we measure the density ρ_{current} of the state we just calculated and compare it with the density ρ_{target} we are targeting. If the condition

$$\frac{|\rho_{\text{current}} - \rho_{\text{target}}|}{|\rho_{\text{target}}|} < \varepsilon_\rho \quad \text{with} \quad \varepsilon_\rho \ll 1 \tag{20}$$

is fulfilled, we keep the chemical potential μ we plugged in, if not, a routine that involves interpolation and extrapolation is used to determine a new chemical potential which is applied from this point on. Second, we measure the value of the MF parameter α from the candidate state and check if it is converged via the condition

$$|\alpha_{\text{ini}} - \alpha_{\text{new}}| \,/\, |\alpha_{\text{ini}}| < \varepsilon_\alpha \quad \text{or} \quad |\alpha_{\text{new}}| < \varepsilon_\alpha \,. \tag{21}$$

If this condition is fulfilled, we keep α, if not, we once again use a routine that involves extrapolation in order to find a new and better value for α. Finally, we are either done if both conditions Eqs. (20) and (21) are fulfilled or we repeat the whole routine using now the new values we obtained for α and μ as a starting point.

A schematic of the self-consistent ground-state search is depicted in Fig. 8.

B Effect of the Time Window for the Ramp

In Sec. 4 it was mentioned that a ramp appeared to be numerically more stable than an instantaneous quench. For a more detailed explanation of this statement, we compare the accuracy of the data we measure for the MF parameter $|\alpha|$ for a quench and a ramp in Fig. 9.

Changing V either through an instantaneous quench or through a fast continuous ramp, the latter of which we have used throughout the main text, we evolve our system up to times of $t_{\text{end}} = 15$. In both cases we compare the variance between the α data for two different bond dimensions χ, as it was done in Sec. 4.2 as a check of accuracy. We find that difference is two orders of magnitude smaller for the ramp compared to the case of the instantaneous quench. This is why we chose to use ramps for all our calculations presented in this paper.

References

[1] J. G. Bednorz and K. A. Müller, Possible high t c superconductivity in the ba- la- cu- o system, Zeitschrift für Physik B Condensed Matter **64**(2), 189 (1986).

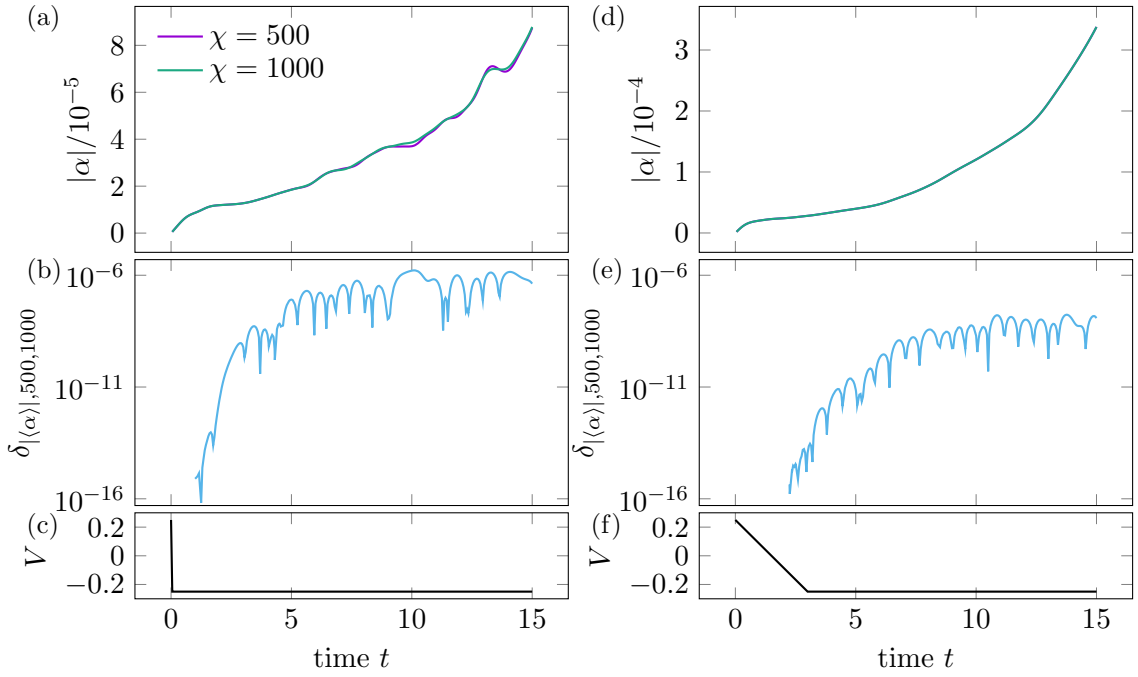

Figure 9: Comparing an instantaneous quench (left hand side) with a fast ramp in finite time (right hand side). Top row showing the time evolution of $|\alpha|$ for two different bond dimensions $\chi = 500$ and $\chi = 1000$ in a 12-site system, bottom row showing the difference between the two bond dimensions. We gain an accuracy of the order of 10^2 via the fast ramp, as opposed to the instant quench.

[2] H. Takagi, S.-i. Uchida, K. Kitazawa and S. Tanaka, High-tc superconductivity of la-ba-cu oxides. ii.–specification of the superconducting phase, Japanese journal of applied physics **26**(2A), L123 (1987).

[3] A. Schilling, M. Cantoni, J. Guo and H. Ott, Superconductivity above 130 k in the hg–ba–ca–cu–o system, Nature **363**(6424), 56 (1993).

[4] E. Dagotto, Correlated electrons in high-temperature superconductors, Reviews of Modern Physics **66**(3), 763 (1994).

[5] J. Hubbard, Electron correlations in narrow energy bands, Proceedings of the Royal Society of London. Series A. Mathematical and Physical Sciences **276**(1365), 238 (1963).

[6] M. C. Gutzwiller, Effect of correlation on the ferromagnetism of transition metals, Phys. Rev. Lett. **10**, 159 (1963), doi:10.1103/PhysRevLett.10.159.

[7] J. Kanamori, Electron correlation and ferromagnetism of transition metals, Progress of Theoretical Physics **30**(3), 275 (1963).

[8] F. H. Essler, H. Frahm, F. Göhmann, A. Klümper and V. E. Korepin, The one-dimensional Hubbard model, Cambridge University Press (2005).

[9] P. Fazekas, Lecture Notes on Electron Correlation and Magnetism, vol. 5 of Series in Modern Condensed Matter Physics, World Scientific Publishing Co Pte Ltd, Singapore (1999).

[10] A. Auerbach, Interacting electrons and quantum magnetism, Springer Science & Business Media (2012).

[11] P. W. Anderson, The resonating valence bond state in la2cuo4 and superconductivity, Science **235**(4793), 1196 (1987), doi:10.1126/science.235.4793.1196, `http://science.sciencemag.org/content/235/4793/1196.full.pdf`.

[12] F. C. Zhang and T. M. Rice, Effective hamiltonian for the superconducting cu oxides, Phys. Rev. B **37**, 3759 (1988), doi:10.1103/PhysRevB.37.3759.

[13] K. A. Chao, J. Spalek and A. M. Oles, Kinetic exchange interaction in a narrow s-band, Journal of Physics C: Solid State Physics **10**(10), L271 (1977).

[14] D. Fausti, R. Tobey, N. Dean, S. Kaiser, A. Dienst, M. C. Hoffmann, S. Pyon, T. Takayama, H. Takagi and A. Cavalleri, Light-induced superconductivity in a stripe-ordered cuprate, science **331**(6014), 189 (2011).

[15] M. Buzzi, D. Nicoletti, M. Fechner, N. Tancogne-Dejean, M. Sentef, A. Georges, T. Biesner, E. Uykur, M. Dressel, A. Henderson et al., Photomolecular high-temperature superconductivity, Physical Review X **10**(3), 031028 (2020).

[16] S. Kaiser, C. R. Hunt, D. Nicoletti, W. Hu, I. Gierz, H. Liu, M. Le Tacon, T. Loew, D. Haug, B. Keimer et al., Optically induced coherent transport far above t c in underdoped yba 2 cu 3 o 6+ δ, Physical Review B **89**(18), 184516 (2014).

[17] M. Mitrano, A. Cantaluppi, D. Nicoletti, S. Kaiser, A. Perucchi, S. Lupi, P. Di Pietro, D. Pontiroli, M. Riccò, S. R. Clark et al., Possible light-induced superconductivity in k 3 c 60 at high temperature, Nature **530**(7591), 461 (2016).

[18] M. Eckstein, M. Kollar and P. Werner, Interaction quench in the hubbard model: Relaxation of the spectral function and the optical conductivity, Phys. Rev. B **81**, 115131 (2010), doi:10.1103/PhysRevB.81.115131.

[19] S. Paeckel, B. Fauseweh, A. Osterkorn, T. Köhler, D. Manske and S. R. Manmana, Detecting superconductivity out of equilibrium, Phys. Rev. B **101**, 180507 (2020), doi:10.1103/PhysRevB.101.180507.

[20] N. Bittner, T. Tohyama, S. Kaiser and D. Manske, Possible light-induced superconductivity in a strongly correlated electron system, Journal of the Physical Society of Japan **88**(4), 044704 (2019).

[21] A. Georges, G. Kotliar, W. Krauth and M. J. Rozenberg, Dynamical mean-field theory of strongly correlated fermion systems and the limit of infinite dimensions, Rev. Mod. Phys. **68**(1), 13 (1996).

[22] H. Aoki, N. Tsuji, M. Eckstein, M. Kollar, T. Oka and P. Werner, Nonequilibrium dynamical mean-field theory and its applications, Rev. Mod. Phys. **86**, 779 (2014), doi:10.1103/RevModPhys.86.779.

[23] P. Bouillot, C. Kollath, A. M. Läuchli, M. Zvonarev, B. Thielemann, C. Rüegg, E. Orignac, R. Citro, M. Klanjšek, C. Berthier, M. Horvatić and T. Giamarchi, Statics and dynamics of weakly coupled antiferromagnetic spin-$\frac{1}{2}$ ladders in a magnetic field, Phys. Rev. B **83**, 054407 (2011), doi:10.1103/PhysRevB.83.054407.

[24] G. Bollmark, T. Köhler, L. Pizzino, Y. Yang, H. Shi, J. S. Hofmann, H. Shi, S. Zhang, T. Giamarchi and A. Kantian, Solving 2d and 3d lattice models of correlated fermions – combining matrix product states with mean field theory (2022), doi:10.48550/ARXIV.2207.03754.

[25] G. Bollmark, N. Laflorencie and A. Kantian, Dimensional crossover and phase transitions in coupled chains: Density matrix renormalization group results, Phys. Rev. B **102**, 195145 (2020), doi:10.1103/PhysRevB.102.195145.

[26] C. Cohen-Tannoudji, J. Dupont-Roc and G. Grynberg, Atom-photon interactions: basic processes and applications (1998).

[27] H. U. R. Strand, M. Eckstein and P. Werner, Nonequilibrium dynamical mean-field theory for bosonic lattice models, Phys. Rev. X **5**, 011038 (2015), doi:10.1103/PhysRevX.5.011038.

[28] I. McCulloch, The matrix product toolkit, Last visit: 21/10/21.

[29] G. Karakonstantakis, E. Berg, S. R. White and S. A. Kivelson, Enhanced pairing in the checkerboard hubbard ladder, Physical Review B **83**(5), 054508 (2011).

[30] M. Dolfi, B. Bauer, S. Keller and M. Troyer, Pair correlations in doped Hubbard ladders, Phys. Rev. B **92**(19), 195139 (2015), doi:10.1103/PhysRevB.92.195139.

[31] T. Giamarchi, Quantum Physics in One Dimension, Oxford University Press (2004).

[32] S. R. White, Density matrix formulation for quantum renormalization groups, Phys. Rev. Lett. **69**(19), 2863 (1992), doi:10.1103/PhysRevLett.69.2863.

[33] S. R. White, Density-matrix algorithms for quantum renormalization groups, Phys. Rev. B **48**(14), 10345 (1993), doi:10.1103/PhysRevB.48.10345.

[34] C. Brockt, F. Dorfner, L. Vidmar, F. Heidrich-Meisner and E. Jeckelmann, Matrix-product-state method with a dynamical local basis optimization for bosonic systems out of equ Phys. Rev. B **92**(24), 1 (2015), doi:10.1103/PhysRevB.92.241106, 1508.00694.

[35] D. Jansen, C. Jooss and F. Heidrich-Meisner, Charge density wave breakdown in a heterostructure with electron-phonon coupling, Phys. Rev. B **104**(19), 1 (2021), doi:10.1103/PhysRevB.104.195116, 2109.07197.

[36] M. Moroder, M. Grundner, F. Damanet, U. Schollwöck, S. Mardazad, S. Flannigan, T. Köhler and S. Paeckel, Metallicity in the dissipative Hubbard-Holstein model: Markovian and non-Markovian tensor-network methods for open quantum many-body systems, doi:10.48550/ARXIV.2207.08243 (2022).

[37] N. Kaushal, J. Herbrych, A. Nocera, G. Alvarez, A. Moreo, F. A. Reboredo and E. Dagotto, Density matrix renormalization group study of a three-orbital Hubbard model with spin-orbit couplin Phys. Rev. B **96**(15), 1 (2017), doi:10.1103/PhysRevB.96.155111, 1707.04313.

[38] M. Klanjšek, H. Mayaffre, C. Berthier, M. Horvatić, B. Chiari, O. Piovesana, P. Bouillot, C. Kollath, E. Orignac, R. Citro and T. Giamarchi, Controlling Luttinger Liquid Physics in Spin Ladders under a Magnetic Field, Phys. Rev. Lett. **101**(13), 137207 (2008).

[39] P. Bouillot, C. Kollath, A. M. Läuchli, M. Zvonarev, B. Thielemann, C. Rüegg, E. Orignac, R. Citro, M. Klanjšek, C. Berthier, M. Horvatić and T. Giamarchi, Statics and dynamics of weakly coupled antiferromagnetic spin- 1 2 ladders in a magnetic field, Phys. Rev. B **83**(5), 054407 (2011), doi:10.1103/PhysRevB.83.054407.